NeuroImage 125 (2016) 208–219

Contents lists available at ScienceDirect

NeuroImage

journal homepage: www.elsevier.com/locate/ynimg

Distinct vestibular effects on early and late somatosensory cortical processing in humans

Christian Pfeiffer [a,b,c], Michiel van Elk [d], Fosco Bernasconi [b,c], Olaf Blanke [b,c,e,*]

[a] Laboratoire de Recherche en Neuroimagerie (LREN), Department of Clinical Neuroscience, Lausanne University and University Hospital, Lausanne, Switzerland
[b] Center for Neuroprosthetics, School of Life Sciences, Ecole Polytechnique Fédérale de Lausanne (EPFL), Switzerland
[c] Laboratory of Cognitive Neuroscience, Brain Mind Institute, School of Life Sciences, Ecole Polytechnique Fédérale de Lausanne (EPFL), Switzerland
[d] Department of Psychology, University of Amsterdam, Netherlands
[e] Department of Neurology, University Hospital Geneva, Switzerland

ARTICLE INFO

Article history:
Received 4 June 2015
Accepted 1 October 2015
Available online 23 October 2015

Keywords:
EEG
Somatosensory evoked potentials
Vestibular system
Multisensory processing
Electrical neuroimaging
Somatosensory cortex

ABSTRACT

In non-human primates several brain areas contain neurons that respond to both vestibular and somatosensory stimulation. In humans, vestibular stimulation activates several somatosensory brain regions and improves tactile perception. However, less is known about the spatio-temporal dynamics of such vestibular–somatosensory interactions in the human brain. To address this issue, we recorded high-density electroencephalography during left median nerve electrical stimulation to obtain Somatosensory Evoked Potentials (SEPs). We analyzed SEPs during vestibular activation following sudden decelerations from constant-velocity (90°/s and 60°/s) earth-vertical axis yaw rotations and SEPs during a non-vestibular control period. SEP analysis revealed two distinct temporal effects of vestibular activation: An early effect (28–32 ms post-stimulus) characterized by vestibular suppression of SEP response strength that depended on rotation velocity and a later effect (97–112 ms post-stimulus) characterized by vestibular modulation of SEP topographical pattern that was rotation velocity-independent. Source estimation localized these vestibular effects, during both time periods, to activation differences in a distributed cortical network including the right postcentral gyrus, right insula, left precuneus, and bilateral secondary somatosensory cortex. These results suggest that vestibular–somatosensory interactions in humans depend on processing in specific time periods in somatosensory and vestibular cortical regions.
© 2015 Elsevier Inc. All rights reserved.

Introduction

The vestibular system contributes to numerous adaptive functions including gaze control (Bertolini et al., 2008), balance (Johansson and Magnusson, 1991; Lacour et al., 1997), self-motion perception (Fetsch et al., 2007; MacNeilage et al., 2007), spatial cognition (Berthoz, 1991) and bodily self-consciousness (Blanke et al., 2002; Lopez et al., 2010). These functions are based on the integration of vestibular signals with multisensory inputs, including visual and somatosensory signals. Although animal research identified several subcortical and cortical structures that process vestibular and multisensory signals (see Lopez and Blanke, 2011 for a review), little is known about the spatio-temporal dynamics of vestibular and multisensory processing in the human brain.

In non-human primates distinct, distributed, and multisensory cortical regions receive vestibular inputs from the thalamus. These include several somatosensory regions, such as the parieto-insular vestibular cortex (PIVC (Chen et al., 2010; Grüsser et al., 1990a,b)) and the primary somatosensory cortex (S1, i.e. Brodmann areas 2v (Büttner and Buettner, 1978; Fredrickson et al., 1966) and 3a (Odkvist et al., 1974)). Vestibular information is further relayed to multisensory regions in the ventral intra-parietal area (Bremmer et al., 2002; Schlack et al., 2002), the middle superior temporal area (Duffy, 1998), as well as other regions (see Guldin and Grüsser, 1998; Lopez and Blanke, 2011 for reviews). This prominent anatomical overlap of somatosensory and vestibular processing (i.e. in PIVC, area 2v, area 3a, and ventral intra-parietal area (Akbarian et al., 1993, 1994; Bremmer et al., 2002; Fredrickson et al., 1966; Guldin et al., 1992; Odkvist et al., 1974; Schwarz and Fredrickson, 1971; Vogt and Pandya, 1978) raises the question whether the vestibular and somatosensory systems might interact at the functional level as well.

This hypothesis has been largely supported by neuroimaging evidence for vestibular–somatosensory interactions in animals and humans. For instance, Fredrickson et al. (1966) described responses from monkey area 2v not only to electrical stimulation of the vestibular nerve, but also to electrical stimulation of the median nerve, or simultaneous stimulation of both nerves. Another study found that subdivisions of monkey area 3a respond to vestibular, proprioceptive, and deep muscle (neck, limbs) stimulation (Odkvist et al., 1974). Similarly, in humans undergoing pre-surgical epilepsy evaluation, direct electro-cortical

* Corresponding author at: Center for Neuroprosthetics, Ecole Polytechnique Fédérale de Lausanne (EPFL), 9 Chemin des Mines, 1202 Geneva, Switzerland. Fax: +41 21 693 69 22.
E-mail address: olaf.blanke@epfl.ch (O. Blanke).

http://dx.doi.org/10.1016/j.neuroimage.2015.10.004
1053-8119/© 2015 Elsevier Inc. All rights reserved.

stimulation of the posterior insula cortex (Mazzola et al., 2014) (i.e. human correlate of the PIVC, Lopez et al., 2012a,b; zu Eulenburg et al., 2012) or the anterior parietal cortex (i.e. human homologue of area 2v) induced vestibular and somatosensory sensations (Blanke et al., 2000; Penfield and Jaspers, 1954).

Overlap of vestibular and somatosensory processing in the human brain has been further demonstrated by functional magnetic resonance imaging (fMRI) and positron emission tomography (PET) studies using caloric (CVS) or galvanic vestibular stimulation (GVS). In these studies, somatosensory and vestibular stimulation activated both the putamen and the secondary somatosensory cortex (S2; Bottini et al., 2005; Bottini et al., 1995) as well as the temporo-parietal junction including the parietal operculum and the medial and posterior insula (Lopez et al., 2012a,b; Mazzola et al., 2014; zu Eulenburg et al., 2012). In these fMRI and PET studies, GVS and CVS further modulated activity in S1 (Bense et al., 2001; Fasold et al., 2002; Lobel et al., 1998; Suzuki et al., 2001). In turn, somatosensory (i.e. proprioceptive) stimulation by neck-muscle vibration has been shown to activate the posterior insula (i.e. PIVC) and the somatosensory cortex (i.e. area 3a and S2; Fasold et al., 2008).

In addition to neuroimaging evidence for vestibular–somatosensory convergence, psychophysical and behavioral studies in humans suggest functional vestibular–somatosensory interactions. In neurological patients with hemianesthesia or tactile extinction, who showed profound somatosensory perception deficits due to damage to the parietal cortex, CVS or GVS temporarily recovered tactile perception (Bottini et al., 1995, 2005; Kerkhoff et al., 2011; Vallar et al., 1990). A similar improvement of tactile detection thresholds at the hands was found in healthy subjects during passive whole-body rotation, GVS, or CVS (Ferrè et al., 2011, 2013, 2014).

Despite the evidence for vestibular–somatosensory neuroanatomical overlap and functional interactions in humans, little is known about the specific spatio-temporal dynamics by which vestibular inputs affect human somatosensory cortical processing. Perhaps, this is due to the limited temporal resolution of fMRI and PET, the constant vestibular activations induced by the static magnetic field of the MR scanner (Roberts et al., 2011), and somatosensory co-activation induced by artificial vestibular stimulation techniques such as CVS and GVS (Lopez et al., 2012a). To address these issues, the main aim of the present study was to identify the spatio-temporal dynamics by which natural vestibular signals affect somatosensory cortical processing in humans. We combined somatosensory evoked potentials (SEPs) with short sequences of constant-velocity passive whole-body yaw rotations that selectively activated the horizontal semicircular canals of the vestibular system (Bertolini et al., 2011; Prsa et al., 2012; van Elk and Blanke, 2013). Based on an earlier study testing the effects of CVS on SEPs (Ferrè et al., 2012), we here recorded SEPs during the post-rotational period (see below), because this period is marked by prolonged vestibular activation (Bertolini et al., 2011; Goldberg and Fernandez, 1971). Critically, because vestibular activation was ongoing after body rotation had stopped, we avoided effects of somatosensory co-activation that accompany the onset of vestibular yaw rotation (Allison et al., 1989a). In addition, because the vast majority of vestibular neurons in animals encode rotation velocity of the head by modulation of response strength (i.e. gain; Barresi et al., 2013; Goldberg and Fernandez, 1971; Waespe et al., 1980) and because humans can accurately discriminate between different rotation velocities based on vestibular inputs alone (Grabherr et al., 2008; Prsa et al., 2012), we asked here whether different rotation velocities would further modulate vestibular–somatosensory interactions. Thus, SEPs were recorded during vestibular activation immediately following decelerations from fast (90°/s) or slow (60°/s) constant-velocity yaw rotations and during a later control period without any vestibular activation. We predicted that any vestibular modulation of the SEP response strength would further depend on rotation velocity. We performed electrical neuroimaging analysis (Murray et al., 2008) and analyzed whether early (Fredrickson et al., 1966; Odkvist et al., 1974) and/or late SEP components (Ferrè et al., 2012) were modulated by vestibular activation and rotation velocity.

Materials and methods

Participants

Sixteen students from the Ecole Polytechnique Fédérale de Lausanne participated (4 females; mean age = 23.8 years, SD = 4.2 years, range = 19–32 years). All participants verbally indicated that they were right-handed, had normal balance and somatosensory perception, and no history of psychiatric or neurologic diseases. Before inclusion in the study each participant gave informed consent and after having participated each participant received a 60 Swiss Francs monetary compensation. The experimental protocol was approved by the local ethics committee—La Commission d'Ethique de la Recherche Clinique de la Faculté et de Medicine de l'Université de Lausanne—and was conducted in accordance with the Declaration of Helsinki.

Experimental setup

Fig. 1A shows a top view of the experimental setup modified from a similar experimental setup used by us in Prsa et al. (2012) and van Elk and Blanke (2013). Inside of a faraday cage (Industrial Acoustics Company, Niederkrüchten, Germany), used to shield the experimental setup from external electromagnetic, visual, and auditory signals, a motion platform was installed. A racing car seat was firmly mounted at the axial center of a beam platform (2 m diameter) that was fixated on an electrical engine (PCI-7352 servo control). Platform rotations were controlled with 0.1 angular degree precision at 100 Hz sampling rate using LABVIEW software (version 8.6, National Instruments, Austin, TX, US).

The participant sat comfortably in upright posture with safety belts attached. The racing car seat had a tight anatomical fit, which both stabilized body position and constrained any involuntary trunk or leg movements during rotation. The participant's head was centered above the trunk and the rotation axis. The participant's head was tilted by 30° forward, which because of the anatomical configuration of the semicircular canals aligned participant's horizontal canals with the yaw rotation plane (Day and Fitzpatrick, 2005). A chin- and forehead-rest were used to stabilize participant's head posture during platform rotation. This setup allowed to apply passive whole-body yaw rotations about an earth-vertical axis through the participant's head center and thus selectively stimulated the horizontal semicircular canals of the vestibular system. Indeed, we cannot exclude inter-subject variability of head position with respect to the rotation axis that may have also led to additional otolith vestibular activation. However, these variations were comparatively small and random between subjects and can, therefore, be considered negligible.

A screen (Samsung Syncmaster 2233RZ, Seoul, Korea) with 120 Hz refresh rate and 22-inch diameter was positioned at eye-level in front of the participant and was firmly attached to the motion platform. The screen had 29 cm eye-to-screen distance giving rise to 56° vertical and 80° horizontal visual angles. A white fixation cross was presented at the center of the screen on a black background. Apart from the fixation cross the experiment was conducted in complete darkness, such that no visual signal informed participants whether the platform rotated or not. Furthermore, the participant wore earphones (Sennheiser CX 400, Hannover, Germany) on which white noise (individually adjusted between 40–70 dB loudness) was presented to mask auditory cues from platform rotations. A computer was laterally mounted on the platform that was used to control the visual display (i.e. presenting instructions and a fixation cross) and for scheduling median nerve stimulations.

An electrical stimulator (Grass S48, Astor-Med Inc., West Warwick, RI, US) was installed laterally on the beam platform and was used to generate electrical currents for median nerve stimulation. The electrical stimulator was connected to an isolation unit (Grass SIU5), a constant

current stimulus unit (Grass CCU1), and to two disk electrodes (GRASS F-E5GH) attached to the skin at the participant's left wrist above the median nerve. Before the experiment participant's skin at the left wrist was cleaned with alcohol and the electrodes were attached with conducting gel in order to reduce skin resistance. Electrode placement was individually adjusted, such that electrical stimulations induced clearly visible thumb abductions. Participants were instructed to place their hand passively palm upwards on a soft cushion on their legs in order to avoid any somatosensory confounding stimulation of the skin innervated by the median nerve during rotations. We note however that electrical median nerve stimulations innervate not only somatosensory-proprioceptive afferents, but also nociceptive fibers (Cruccu et al., 2008). In order to prevent painful sensations related to median nerve stimulation, we here used motor threshold stimulus intensities known to cause only mild discomfort (Cruccu et al., 2008). This was confirmed by informal repeated inquiry of our subjects before and in-between experimental blocks: No subject reported painful or noxious sensation related to median nerve stimulation or rotation stimuli. Importantly, because this median nerve stimulation intensity was constant throughout the experiment, and hence across experimental conditions, we can exclude that noxious or painful sensations contributed to our results or explain statistical differences observed between experimental conditions.

Experimental design, procedure and stimuli

The experimental manipulations were based on a 2 × 2 × 2 full-factorial experimental design with the within-subjects factors Condition (vestibular activation, control), Rotation Velocity (fast, slow), and Rotation Direction (clockwise, counterclockwise). However, the main goal of this study was to identify the effects of Condition and Rotation Velocity on somatosensory cortical processing (using a 2 × 2 experimental design). Therefore, we randomized the rotation direction from trial to trial in order to reduce anticipation effects (Bertolini et al., 2008; Prsa et al., 2012; van Elk and Blanke, 2013). After all experimental data was recorded and processed (see below) we conducted initial statistical analysis to evaluate effects of Rotation Direction on our data. We thus performed all analyses mentioned in the Analysis section using the three-factorial design. Because the results of these analyses showed no main effects or interactions with the Rotation Direction factor, in the following we present the experimental setup and analysis for a pooled experimental design with 2 (Condition: vestibular activation, control) × 2 (Rotation Velocity: fast, slow) experimental factors.

Fig. 1B–C shows the general sequence of events of an experimental rotation trial. Steps of same-duration (32 s) constant-velocity rotation were used in order to induce post-rotational vestibular activation, i.e. that is vestibular activation while the body (and the motion platform) did not move (Bertolini et al., 2011). Initially, the motion platform was static (0°/s velocity) and accelerated during 1 s to maximum velocity (90°/s in the fast condition, 60°/s in the slow condition) with a cosine-smoothed acceleration profile (Gaussian shape) reaching at 500 ms after rotation onset the maximum acceleration (180°/s^2 in the fast condition, 120°/s^2 in the slow condition). This was followed by constant rotation at maximum velocity (i.e. 90°/s or 60°/s according to the experimental condition) during 30 s. It is known that during constant-velocity rotation, horizontal canal activity habituates over time following an approximately exponential decay with 15–20 s time constant (Bertolini et al., 2011; Raphan et al., 1979). Thus, at the end of the constant-velocity rotation there was a minimal amount of vestibular activation and no residual peripheral semicircular canal activation (i.e. time constant of 4–6 s Büttner and Waespe, 1981; Cohen et al., 1981; Goldberg and Fernandez, 1971). This was followed by rapid platform deceleration from maximum velocity to no-motion (0°/s) during 1 s by means of a cosine-smoothed profile that was the reverse of the profile used for platform accelerations. Such rapid changes in velocity (i.e. accelerations) induce, similar to the initial platform acceleration, prolonged vestibular activation (time constant of 15–20 s; Bertolini et al., 2011; Cohen et al., 1981; Laurens and Angelaki, 2011; Raphan et al., 1979) while the body does not move. In fact, electrophysiological recordings and mathematical models of the vestibular system strongly suggest that using such angular rotation profiles, peri-rotational (following platform acceleration) and post-rotational (following platform deceleration) vestibular activations are identical (Bertolini et al., 2011; Goldberg and Fernandez, 1971; Laurens and Angelaki, 2011).

Fig. 1C shows the sequence of events with two time intervals following a rotation when SEPs were acquired. First, immediately following the sudden platform decelerations, i.e. during post-rotational vestibular activation, 80 subsequent median nerve stimulations were presented at 4-Hz frequency with a fixed 250-ms inter-stimulus interval for 20 s (vestibular activation condition). Triggers associated with the onset of median nerve stimulation were sent in parallel to the EEG computer for post-hoc analysis of SEPs. Electrical median nerve stimulations were transcutaneous constant-current square wave pulses of 0.15 ms duration and 8–12 mA intensity individually adjusted to 110% of motor threshold (i.e. visible thumb abductions) known to be 3–4 times higher than perceptual threshold (Mauguiere, 2005) and innervating both tactile, proprioceptive, as well as nociceptive afferents of the median nerve (Cruccu et al., 2008). This was followed by a resting period during which no stimulus was presented and vestibular activation habituated during 32 s. Immediately after that, i.e. during no vestibular activation, another series of 80 median nerve stimulations with identical parameters from the first stimulation interval was presented during 20 s (control condition). The total duration of a rotation trial was thus 104 s. Each participant was presented with 12 rotation trials in 2 separate sessions of 6 subsequent rotation trials. A total of 1.920 median nerve stimulations were presented to each participant with 480 stimulations per experimental condition, i.e. (1) vestibular activation & fast rotation, (2) vestibular activation & slow rotation, (3) control & fast rotation, and (4) control & slow rotation conditions.

We note that inertial forces during the rotation deceleration phase might have induced low-intensity somatosensory inputs (due to changes of contact pressure between the rotating chair and the participant's legs and trunk). We cannot exclude that the cortical processing induced by those mild leg/trunk somatosensory inputs might have continued after rotation stop and therefore might have contributed partially to our SEPs recorded immediately after the rotation had stopped. However, our SEP recordings and analyses were exclusively performed when the motion platform was stable to avoid confounding somatosensory inputs induced by the platform rotations and making the contribution of such inputs to the SEPs (recorded for a prolonged period of 20 s after rotation stop) unlikely.

In addition, after having completed the SEP recordings following constant-velocity rotation reported in this manuscript, participants completed another separate EEG recording session consisting of SEP recordings during the acceleration and deceleration phases of short (2 s) transient yaw rotations. Unfortunately, these other data could not further be reported, because SEPs were too strongly contaminated by artifacts from rotational accelerations and decelerations.

EEG data acquisition and preprocessing

Continuous EEG was acquired at 2048 Hz with a 64-channel Biosemi ActiveTwo system (Biosemi, Amsterdam, Netherlands, www.biosemi.nl) referenced to a vertex CMS-DRL ground, which serves as a feedback loop driving the average potential across all channels as close as possible to the amplifier zero. During EEG preparation for each participant the experimenters took care to keep DC offsets below 50 mV for all channels (i.e. for active EEG recording systems DC offset serves as evaluation criterion similar to channel impedances for passive montages). All data was recorded with an online 0.2–100 Hz band-pass filter.

Offline data pre-processing was conducted using EEGLAB software (http://sccn.ucsd.edu/eeglab/), the FASTER toolbox (http://www.mee.

tcd.ie/neuraleng/Research/Faster) implemented in MATLAB software (MathWorks, version R13, http://www.mathworks.ch) and customized MATLAB scripts. In order to correct for slight temporal imprecisions (i.e. on average < 5 ms) between computer-scheduled triggers and actual median nerve stimulus onsets, which might have affected the interpretation of early short-latency SEP components, we initially identified in the continuous EEG data for each scheduled event (i.e. stimulation trigger) the related electrical stimulation artifact onset, which became clearly apparent as a short-latency (<5 ms) and high amplitude (>50 mV) electrical artifact in all scalp channels (e.g. see brief waveform deflection by the electrical artifact immediately after stimulus onset in Fig. 2A–B). After having in this way identified stimulation artifact onset latencies we assigned those empirically identified latencies to the stimulus onset triggers further used for evoked potential analysis. Then, continuous raw data was high-pass filtered (1 Hz low cut-off, ripple: 0.05 dB, attenuation: 80 dB, transition bandwidth: 0.5 Hz) and notch filtered (48–52 Hz, bandwidth: 3 dB, ripple: 0.05 dB, attenuation: 80 dB, transition bandwidth: 1 Hz) using second-order Butterworth filters. The data was recalculated against the average reference. Artifact electrodes from each participant were identified using a signal variance criterion (3 z-score Hurst exponent). On average, 6 (SD = 3) electrodes were interpolated for each participant using spherical splines (Nolan et al., 2010).

EEG epochs from −50 to 200 ms relative to stimulus onset (i.e., median nerve stimulation) were extracted for each participant and each condition. A pre-stimulus baseline correction from −50 to 0 ms pre-stimulus onset was applied. Physiological artifacts (e.g. muscular artifacts, eye blinks) were removed by semi-automated procedures including independent component analysis (ICA; 63 components, k-value: 25, kurtosis rejection criterion: 3 z-scores), application of a ±100 μV bipolar vertical EOG signal rejection criterion, and by visual inspection. The average percentage (and standard deviation) of rejected epochs per subject was 19 (14) percent and the average number (and standard deviation) of accepted epochs per experimental condition was 415 (63) epochs for vestibular activation-fast rotation velocity, 365 (55) epochs for vestibular activation-slow rotation velocity, 414 (65) epochs for control-fast rotation velocity and 364 (58) epochs for control-slow rotation velocity. Statistical analysis using a repeated-measures ANOVA on the accepted number of epochs per condition for the participant sample showed no significant main effects or interactions related to the Condition and Rotation Velocity factors (all p-values > 0.1). Thus, we can exclude that our results were due to differences in signal to noise ratio across conditions. For each subject condition-wise averages were calculated (i.e. SEPs) and subjected to further statistical analysis.

EOG data acquisition and analysis

In order to quantify possible eye movement artifacts during the SEP period, bipolar horizontal electrooculography (EOG) was recorded from additional electrodes attached to the outer canthi and bipolar vertical EOG was recorded from electrodes above and below the right eye. EOG data were acquired at 2048 Hz simultaneously with EEG data via the Biosemi ActiveTwo system. The EOG data was filtered using a high-pass (1 Hz cut-off) and a notch (48–52 Hz) second-order Butterworth filter. Subsequently, EOG data was segmented into −50 to 200 ms epochs relative to median nerve stimulus onset. Epochs locked to median nerve stimulation onset from the four experimental conditions were subjected to a 2 (Condition: vestibular activation, control) × 2 (Rotation Velocity: fast, slow) within-subjects repeated measures ANOVA. There were no main effects of Condition and Rotation Velocity, and no Condition × Rotation Velocity interaction (all p-values > 0.05). We found no Condition main effect, indicating that participants successfully suppressed the vestibular ocular reflex to maintain fixation (vestibular activation condition was indistinguishable from non-vestibular control condition where no eye movements were expected). This is further supported by the observation that during data pre-processing a similar amount of epochs was rejected (based on EOG amplitude thresholds) for the vestibular activation and control conditions (see above).

EEG analyses and source estimation

The effects of vestibular activation on somatosensory processing were identified using a step-wise analysis procedure, which hereafter will be referred to as electrical neuroimaging analysis. Electrical neuroimaging analysis was conducted using CARTOOL software (Functional Brain Mapping Laboratory, Geneva, Switzerland http://www.brainmapping.unige.ch/cartool.htm), STEN software (Laboratory of Investigative Neurophysiology, Lausanne, Switzerland, http://www.unil.ch/line/Sten), RAGU software (http://www.thomaskoenig.ch/Ragu_pkg.exe), and customized scripts in MATLAB software.

Electrical neuroimaging analysis allowed us to assess and differentiate the effects of strength modulations (i.e. modulations in global field power, GFP) that occurred in the absence of topographic modulations (i.e. modulations in global map dissimilarity, GMD) that resulted from changes in the intracranial source configuration. Because each step of the electrical neuroimaging analyses is independent from the others, any combination of these neurophysiologic phenomena can be assessed (Murray et al., 2008). Finally, we used the local autoregressive average distributed linear inverse solution (LAURA, Grave de Peralta Menendez et al., 2001) to estimate the intracranial sources of the neurophysiologic effects identified in the previous steps of the electrical neuroimaging analysis (GFP and/or GMD modulations).

Global electrical field analysis

Two reference electrode-independent analyses of the global electrical field strength (i.e. GFP, Murray et al., 2008) and topographical changes (i.e. GMD, Koenig and Melie-Garcia, 2010) were conducted. GFP is calculated as the square root of the mean of the squared values recorded at each electrode (versus average reference) and represents the spatial standard deviation of the potentials at all electrodes and at each time point (Lehmann and Skrandies, 1980). This measure indicates the global strength of the response, regardless of its topographic distribution. Changes in GFP were statistically analyzed at each time point from −50 to 200 ms relative to stimulus onset using repeated-measures ANOVAs with the within-subjects factors Condition (vestibular activation, control) and Rotation Velocity (fast, slow) with an alpha threshold of $p < 0.05$. To control for multiple comparisons and temporal autocorrelation, we applied in our GFP analysis a >11-contiguous data-point criterion for the persistence of differential statistical effects (Guthrie and Buchwald, 1991) for the entire −50 ms to 200 ms peristimulus interval (i.e. 512 data points). In addition, in line with the proposal that GFP peaks reflect periods of highest functional and topographical stability (Lehmann and Skrandies, 1980; Pascual-Marqui et al., 1995), statistical analysis of GFP in periods-of-interest was conducted by first identifying in the group-average GFP the prominent positive GFP peaks by visual inspection, based on which time windows were defined (i.e. at 28–32 ms, 44–48 ms, and 64–68 ms post-stimulus). Then, period-of-interest-wise condition-average GFP data were calculated for each subject and these data were statistically analyzed by separate two-way repeated-measures ANOVAs (i.e. same factors as for time-wise analyses; alpha threshold of $p < 0.05$).

Topographic modulations across conditions were identified using GMD (Koenig and Melie-Garcia, 2010), which is calculated as the root mean square of the differences between two strength-normalized vectors (i.e. instantaneous voltage potentials across the electrode montage). The GMD values between four experimental conditions (i.e. factorial combinations of Condition and Rotation Velocity experimental factors) were then compared at each time point with an empirical distribution derived from a bootstrapping procedure (5000 permutations per data point, alpha threshold of $p < 0.05$) based on randomly

reassigning each participant's data to either one of the four experimental conditions. Similar to the GFP analysis we applied for the GMD analysis a >11-contiguous data-point criterion for the persistence of statistical effects (Guthrie and Buchwald, 1991) for correcting for multiple comparisons and temporal auto-correlation. GMD is independent of the chosen reference electrode and is insensitive to pure amplitude modulations across conditions, i.e. that is GMD modulations are orthogonal to GFP modulations. The combination of GFP and GMD analyses is useful in terms of the neurophysiologic interpretability, following the assumption that topographic changes necessarily reflect differences in the configuration of the brain's underlying active generators (Lehmann and Skrandies, 1980).

Topographical pattern differences, as revealed by GMD analysis, were further evaluated by microstate pattern analysis, using an initial step (i.e. topographical segmentation) based on hierarchical clustering using an atomize and agglomerate approach and was performed over contiguous 0–200 ms post-stimulus interval to identify the pattern of predominating topographies (template maps) in the cumulative group averaged data (Murray et al., 2008). This serves as hypothesis generation tool that is subsequently statistically evaluated using single-subject data. Thus, here we focused on the time periods where significant GMD differences were observed. Within these time periods, differences in the pattern of maps observed during topographical segmentation between conditions in the group-average data were tested by calculating the spatial correlation between these maps from the group-average data and each time-point of single-subject (referred to as individual subject fitting). This allows extracting the duration of presence of each topographical map (in ms) in the time interval of interest (i.e. 16 subjects × 2 factor levels for Condition × 2 factor levels for Rotation Velocity). Statistical analysis of map presence was performed using a 2 × 2 repeated measures ANOVA for each topographical map.

Source estimations

To identify the intracranial sources generating the GFP and GMD effects, over distinct time periods, we estimated the electrical activity in the brain using a distributed linear inverse solution applying the local autoregressive average regularization approach (LAURA), comprising biophysical laws as constraints (Grave de Peralta Menendez et al., 2001; Michel et al., 2004). For the lead field matrix calculation, we applied the spherical model with anatomical constraints (SMAC) method (Spinelli et al., 2000), which transforms a standard anatomical MRI to the best-fitting sphere using homogeneous transformation operators. It then determines a regular grid of 3005 solution points in the gray matter of this spherical MRI and computes the lead filed matrix using the known analytical solution for a spherical head model with three shells of different conductivities as defined by (Ary et al., 1981). The results of the global electrical field analysis described above provide an estimation of the two distinct time intervals for conducting separate source estimations. Intracranial sources were statistically compared at each node level using the same 2 (Condition: vestibular activation, control) × 2 (Rotation Velocity: fast, slow) repeated measures ANOVA ($p < 0.05$ and at least 8 contiguous nodes) within-subjects design as used for global electrical field analysis. The results of the statistical analysis of source estimations were rendered on the Montreal Neurologic Institute's average brain with the Talairach and Tournoux (1988) coordinates.

Results

In order to allow comparison to previous SEP studies, exemplar single-electrode SEP waveforms for all four experimental conditions are shown in Fig. 2A. However, all interpretations of experimental results in this study are based on global electrical field analysis and source estimation based on the waveforms recorded from the total 64 EEG electrodes.

Global electrical field analysis

Period-of-interest analysis of GFP (Fig. 2B) revealed a significant Condition × Rotation Velocity interaction in the 28–32 ms post-stimulus interval ($F(1,15) = 9.03$, $p < 0.01$, $\eta^2 = 0.38$). Fig. 2D shows the average GFP amplitude for the 28–32 ms post-stimulus interval as a function of experimental condition. Over the 28–32 ms post-stimulus period the GFP amplitude was lower during vestibular activation following fast Rotation Velocity as compared to slow Rotation Velocity (paired-samples t-test: $t(15) = -2.07$, $p < 0.05$) and the

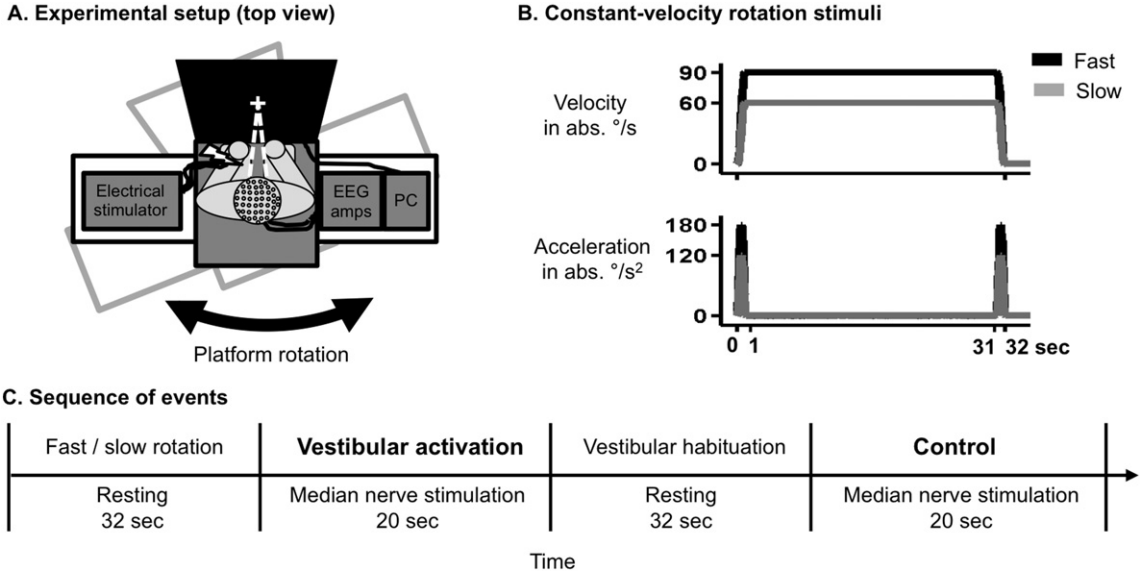

Fig. 1. Experimental setup and procedures. (A) Experimental setup viewed from the top showing the participant (image center) equipped with electroencephalography (EEG) recording electrodes (black dots) and median nerve stimulation electrodes (white flash). The participant was seated at the center of an angular motion platform (white rectangle) on which an electrical stimulator, EEG amplifiers (amps), stimulation computer (PC) and a computer screen (black trapezoid) were firmly attached. The participant fixated a central cross (white) presented on the computer screen throughout the experiment. (B) Platform motion kinematics over time consisted of 30-s steps of 90°/s (fast rotation; in black) or 60°/s (slow rotation; in gray) constant-velocity rotation. (C) Sequence of events of a rotation trial. Immediately following deceleration from constant-velocity rotation during vestibular stimulation and during a later non-vestibular control period, EEG was recorded to median nerve stimulations in trains of 20-s stimulation at 4 Hz (fixed 250-ms inter-stimulus interval).

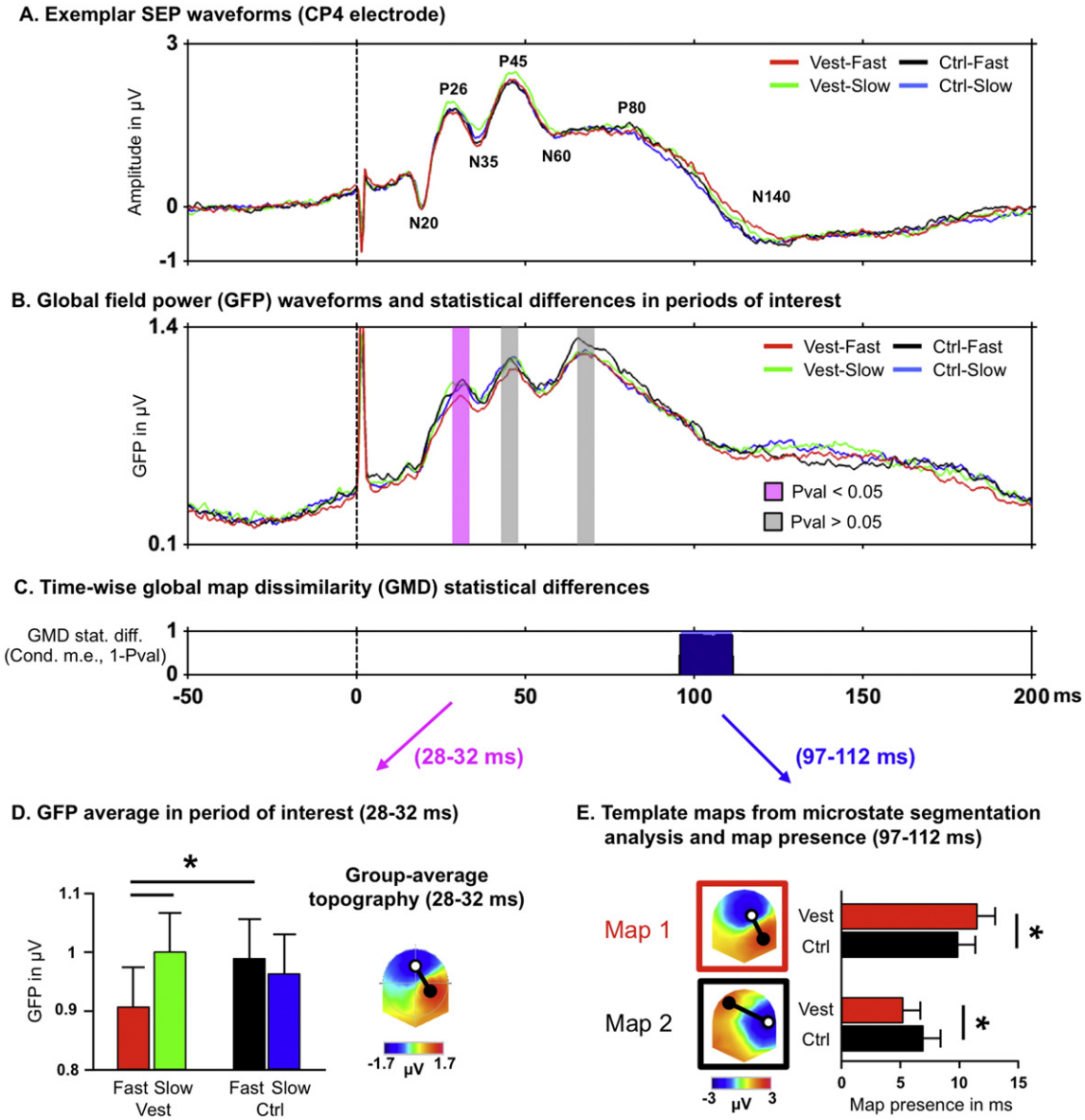

Fig. 2. Electrical neuroimaging results. (A) Group averaged (n = 16) somatosensory evoked potentials (SEPs) to left median nerve stimulations for exemplar electrode CP4 in for all experimental conditions. Waveform peaks (P) and troughs (N) are labeled according to their latency (number) relative to stimulus onset. Blue and pink highlight reflect significant differences identified by global electrical field analysis (see below). (B) Global field power waveforms across time for all experimental conditions and results of GFP-peak period-of-interest statistical analysis ($p < 0.05$, in pink; $p > 0.05$, in gray). (C) Time-wise repeated measures ANOVA results on global map dissimilarity (GMD) ($1 - p$-value shown) are shown for time periods meeting at least 12 contiguous data points. The GFP analysis revealed a significant Condition × Rotation Velocity interaction ($p < 0.05$; in green) from 28–32 ms. The GMD analysis revealed a significant Condition main effect ($p < 0.05$; in purple) from 97–112 ms. (D) Barplot shows global field power average over the 28–32 ms period as a function of experimental condition and post-hoc t-test significant differences are marked (*, $p < 0.05$). Group-average topography (nasion upward) of the potential field across conditions over the 28–32 ms period with positive (black circle) and negative (white circle) peak electrodes. (E) Segmentation analysis over the 97–112 ms period revealed two topographical maps (nasion upward, peak electrodes highlighted by circles) that differentially accounted for the vestibular stimulation (Map 1; in red) and the non-vestibular control (Map 2; in black) conditions. This was revealed by individual subject fitting analysis consisting of individual condition-wise extraction of map presence during the 97–112 ms period and subsequent repeated measures ANOVAs showing for each map significant main effects of Condition (* $p < 0.05$).

control condition (vestibular activation & fast rotation vs. control & fast rotation: $t(15) = -2.05$, $p < 0.05$). There was no difference in GFP between the two control conditions (control & fast rotation vs. control & slow rotation: $t(15) = 0.68$, $p = 0.52$). These results reveal a vestibular modulation of the SEP global electrical field strength that was rotation velocity-dependent and only followed our fast constant-velocity rotation. The GFP analysis in the same time period showed no main effect of Condition ($F(1,15) = 0.34$, $p = 0.57$, $\eta^2 = 0.02$), no main effect of Rotation Velocity ($F(1,15) = 0.94$, $p = 0.35$, $\eta^2 = 0.06$). No main effects of Condition, Rotation Velocity and no Condition × Rotation Velocity interaction were observed in the 44–48 ms and the 64–68 ms post-stimulus

Table 1
Source estimation results (28–32 ms).

Region	Side	x	y	z	BA
Supramarginal gyrus	Right	54	−38	32	40
Middle temporal gyrus	Right	48	−67	22	39
	Right	51	−49	−8	37
	Left	−60	−48	1	22
Precuneus	Left	−9	−70	35	7

Local maxima (Talairach coordinates) of significant clusters (Condition × Rotation Velocity interaction, $p < 0.05$, at least 8 contiguous nodes) from node-wise statistical analysis; BA, Brodmann area.

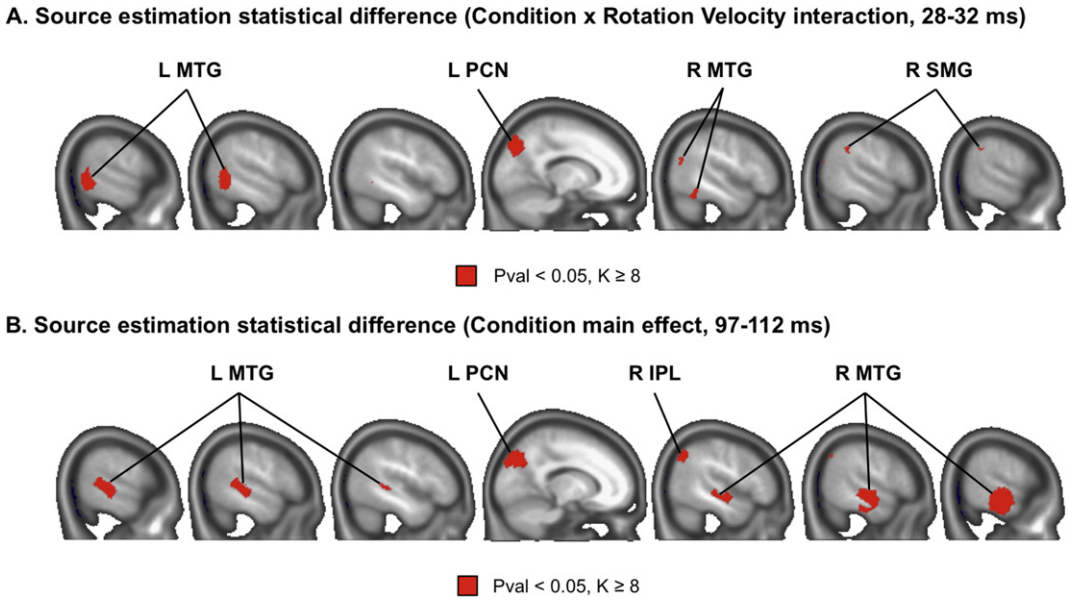

Fig. 3. Node-wise source estimation statistical differences for the (A) Condition × Rotation Velocity interaction in the 28–32 ms post-stimulus interval and for the (B) Condition main effect in the 97–112 ms post-stimulus interval ($p < 0.05$ and at least 8 contiguous nodes). Abbreviations: R: right hemisphere, L: left hemisphere; MTG: middle temporal gyrus, PCN: precuneus, SMG: supramarginal gyrus, IPL: inferior parietal lobe.

periods of interest and for time-wise analysis of GFP over the −50 ms to 200 ms peri-stimulus interval (i.e. no > 11 contiguous data points had p-values < 0.05).

Next we performed time-wise topographical pattern analysis. This GMD analysis revealed no statistically significant main effects or interactions in the early periods (<50 ms; p-values > 0.1), including the 28–32 ms post-stimulus period that had revealed vestibular effects on GFP. This suggests that early stages of somatosensory cortical processing show no changes in topographical pattern (i.e. no statistical changes in the configuration of the underlying neural generators) related to our experimental manipulations. For later time periods (>50 ms), the same GMD analysis revealed a Condition main effect in the 97–112 ms post-stimulus interval (p-values < 0.05; Fig. 2C). To assess the topographical configurations underlying this difference we performed microstate pattern analysis of the group average SEPs for this period in each condition. This analysis revealed two different SEP maps in the 97–112 ms post-stimulus interval (Fig. 2E) that were confirmed by statistical analysis of these two topographical maps (individual subject fitting) in the 97–112 ms period. This analysis revealed that Map 1 accounted more for the vestibular activation condition ($p < 0.05$) and Map 2 accounted more for the control condition ($p < 0.05$; Fig. 2E). Apart from this Condition main effect in the 97–112 ms post-stimulus period, the GMD analysis revealed no Rotation Velocity main effect and no Condition × Rotation interaction (p-values > 0.05; results not shown).

To summarize, the electrical neuroimaging analysis revealed two distinct time periods during which vestibular activation modulated SEPs. We found a rotation velocity-dependent vestibular modulation of SEPs during an early period (i.e. 28–32 ms) without any changes in the underlying neural generators and a rotation velocity-independent vestibular modulation of SEPs during a later period (i.e. 97–112 ms) that revealed the presence of different neural generators for vestibular activation versus control conditions (i.e. without any significant global electrical field strength modulations).

Table 2
Source estimation results (97–112 ms).

Region	Side	x	y	z	BA
Inferior parietal lobe	Right	45	−63	46	40
Middle temporal gyrus	Right	66	−22	−8	21
	Left	−49	−32	0	21
Precuneus	Left	−9	82	41	19

Local maxima (Talairach coordinates) of significant clusters (rotation main effect, $p < 0.05$, at least 8 contiguous nodes) from node-wise statistical analysis; BA, Brodmann area.

Source estimation analysis

LAURA distributed source estimations of SEPs were calculated over the 28–32 ms post-stimulus period where GFP analysis revealed modulations of the global electrical field strength (i.e. Condition × Rotation Velocity interaction) and over the 97–112 ms post-stimulus period where GMD analysis revealed topographical pattern differences (i.e. Condition main effect). Source estimation analysis of the early 28–32 ms post-stimulus interval showed a significant Condition × Rotation Velocity interaction ($p < 0.05$ and at least 8 contiguous nodes) in three different regions: right supramarginal gyrus, bilateral middle temporal gyrus (MTG), and left precuneus (Fig. 3A; Table 1 lists Brodmann area (BA) numbers and Talairach coordinates for these regions).

Statistical analysis of source estimations from the late period (97–112 ms post-stimulus interval) showed a significant Condition main effect ($p < 0.05$ and at least 8 contiguous nodes) that was localized to three very similar regions as in the early 28–32 ms post-stimulus interval: right inferior parietal lobe, bilateral MTG, and right precuneus (Fig. 3B; BA numbers and Talairach coordinates in Table 2). In addition, in both early 28–32 ms and late 97–112 ms post-stimulus time periods additional regions showed statistical differences (p-values < 0.05), which however did not reach the cluster criterion (at least 8 contiguous nodes) for multiple comparison corrections. These regions were the right postcentral gyrus (BA 2; Talairach coordinates: 55, −27, 43), and right posterior insula (BA 13; coordinates: 43, −17, 4).

Discussion

Using natural vestibular activation following passive whole-body yaw rotation and concurrent median nerve SEP recordings we assessed the spatio-temporal brain dynamics of vestibular–somatosensory interaction. We observed two distinct temporal effects of vestibular activation on somatosensory cortical processing, one early effect (i.e. 28–32 ms post-stimulus period) and a later effect (i.e. 97–112 ms post-stimulus period) localized to distributed cortical regions. Our approach, combining EEG with natural vestibular activation, sheds light on the

temporal dynamics of vestibular–somatosensory interaction in humans and extends previous fMRI and PET studies that had identified the brain regions of vestibular–somatosensory interaction in humans (Bense et al., 2001; Bottini et al., 1994, 2001; Fasold et al., 2008). In the following we will discuss both temporal effects separately with respect to previous animal electrophysiology and human neuroimaging data.

Early rotation velocity-dependent vestibular modulation of SEPs

The early vestibular effect on SEPs was rotation velocity-dependent and consisted of a suppression of the SEP global electrical field strength (GFP) following fast (90°/s), but not slow (60°/s) constant-velocity rotation. Although the slow and fast rotation velocities used in our study are known to both activate the semicircular canals (Goldberg and Fernandez, 1971) and to induce self-motion perception above perceptual threshold (Grabherr et al., 2008), vestibular activation differed in intensity between both rotation profiles with the 90°/s profile activating vestibular neurons more strongly (Goldberg and Fernandez, 1971). The early vestibular effect on somatosensory processing is thus more specific than the later effect (see below) as the effect was velocity-dependent and more strongly suppressed in the fast versus slow velocity and this only in the vestibular activation and not in the control condition. Thus, the firing rates of neurons in the vestibular nucleus and the vestibular cortex have been reported to increase with higher head motion velocity (Barresi et al., 2013; Goldberg and Fernandez, 1971; Waespe et al., 1980) and post-rotational nystagmus as well as self-motion sensations are more pronounced during higher rotation speeds (Bertolini et al., 2011). Accordingly, the fast 90°/s yaw rotations used in our study likely induced stronger post-rotational vestibular activation than the slower 60°/s yaw rotations, resulting in a stronger suppression of the SEPs for fast compared to slow rotations. Alternatively, it is known that the duration of post-rotational vestibular activation is variable (Laurens and Angelaki, 2011; Laurens et al., 2013; Raphan et al., 1979) and may have been shorter during slow vestibular constant-velocity rotation, and thus leading to weaker SEP suppression in the 60°/s versus 90°/s rotation velocity trials. As such, we cannot distinguish whether the intensity of vestibular activation or the duration of the vestibular activation in the post-rotatory period (or both) contributed to our results, which will be an important issue to address in future studies.

Next, source estimations for the 28–32 ms post-stimulus period showed that the suppression of SEP amplitude by vestibular stimulation observed at the scalp was associated with brain activation changes in the postcentral gyrus and insular cortex, as well as supramarginal gyrus, precuneus, and MTG (i.e. attributed to S2; see below). The postcentral activation and modulation across conditions was localized in the right postcentral gyrus and, at this SEP latency, likely reflects S1 activation contralateral to the simulated median nerve as expected based on previous SEP studies using surface EEG recordings in humans (Heydrich et al., 2010; Waberski et al., 2002). The postcentral location of this source estimation is also compatible with intracranial recordings in humans revealing the first cortical response to median nerve stimulation in the 20–35 ms post-stimulus period in S1, likely areas 3b and 1 (Allison et al., 1989a). Tracer studies in monkeys showed that both latter S1 sub-regions are reciprocally connected with areas 2v and 3a that are also sub-regions of S1 and both part of the inner circuit of the vestibular cortex (i.e. the interconnected cortical regions receiving direct thalamo-cortical vestibular input; Guldin et al., 1992). Moreover, areas 2v and 3a receive rotational vestibular input and have been reported to respond to median nerve somatosensory signals (in monkeys) similar to those applied in our study (Fredrickson et al., 1966; Odkvist et al., 1974). Given the spatial resolution of EEG we note that we cannot distinguish whether vestibular activation during the early effect modulated activation only in areas 3b/1, only in areas 3a/2v, or in all areas jointly, or even involved areas outside S1 (Michel et al., 2004). However, comparing our data with those obtained by electrophysiological recordings from monkey area 2v (Fredrickson et al., 1966) and given the lateral and posterior extension of the present cluster, we speculate that the present vestibular–somatosensory interaction during the early period originates from activation of the human homologue of area 2v (Bense et al., 2001; Blanke et al., 2000; Fasold et al., 2008; Lobel et al., 1998). This is suggested by some of the results obtained by Fredrickson et al. (1966) who found in monkeys that concurrent electrical stimulation of the vestibular and the median nerve suppressed activity in area 2v (compared to the sum of activity to both unimodal stimulations). Moreover, repeated or delayed stimulation drastically decreased the response of vestibular neurons in area 2v. In line with these data we found a vestibular suppression of SEPs when median nerve stimulation immediately after the sudden platform decelerations, but not during later non-vestibular control period, in our study. Our finding of SEP suppression by vestibular activation is further substantiated by findings in fMRI showing a decreased BOLD signal in S1 following GVS (Bense et al., 2001). However, because GVS also induces nociceptive somatosensory activation, our results extend the findings by (Bense et al., 2001), because the vestibular effects observed in our study were not confounded by the unavoidable somatosensory GVS-related co-activations (Lopez et al., 2012a).

Source estimations for the early 28–32 ms interval further showed statistical differences in the right posterior insula, compatible with previous data implicating this region in vestibular processing. Thus, it has been shown that electro-cortical stimulation of the posterior insula evoked rotational vestibular sensations and somatosensory sensations, whereas stimulation of other parts of the insula induced translational, unspecific, or no vestibular sensation (Mazzola et al., 2014). In monkeys, the posterior insula cortex (i.e. PIVC) responds to somatosensory and vestibular inputs (Grüsser et al., 1990a,b) and is considered in monkeys and humans a core vestibular cortical input region (Guldin and Grüsser, 1998; Lopez et al., 2012a; zu Eulenburg et al., 2012). The insular recruitment in the present study was found in the right hemisphere; we speculate that this is due to the application of left median nerve stimulation recruiting mostly right hemispheric somatosensory responses at this early latency. However, this right-hemispheric lateralization may also be related to the right-handedness of all participants because a previous PET study found that CVS induced ipsilateral-dominant cortical activation with respect to subject's handedness (Dieterich et al., 2003). However, the functional relationship between handedness and vestibular processing is currently unknown, and cannot be explained by the bilateral vestibular peripheral system, by several subcortical crossings of the ascending vestibular pathways, or by bilateral vestibular projections to the cortex (for a review see Dieterich and Brandt, 2015).

Our analysis also revealed an early vestibular effect on somatosensory processing in three additional cortical regions: left precuneus, right supramarginal gyrus, and bilateral MTG (similar to source estimation results of the late period and thus discussed in more detail in the next section). The precuneus shows strong functional connectivity to several vestibular–somatosensory convergence zones as identified in previous studies. These include anatomical connections between precuneus and S1 (i.e. area 2) and S2 cortices (Margulies et al., 2009), as well as precuneus connections to the putative human homologues of the PIVC (posterior insula, parietal operculum; see (Lopez et al., 2012a; zu Eulenburg et al., 2012) for meta analyses). Functionally, the human precuneus belongs to networks involved in higher vestibular functions (Brandt et al., 2014), such as self-motion perception, spatial navigation and spatial memory (Cavanna and Trimble, 2006; Margulies et al., 2009). Thus, our results suggest that the precuneus might contribute to these higher vestibular functions by constantly receiving and processing vestibular and somatosensory inputs, even if such stimulations are applied passively and unrelated to navigation or memory tasks.

Late rotation velocity-independent vestibular modulation of SEPs

Our results also revealed a second time period of vestibular–somatosensory interaction and showed that vestibular activation modulated

SEPs during the later 97–112 ms post-stimulus period. However, the late effect differed from the early effect and we observed differences in the topographical pattern (i.e. GMD) between vestibular activation versus control conditions but found that the response strength (i.e. GFP) was similar across conditions (Bernasconi et al., 2011). This suggests that different neural generators were activated in vestibular activation versus control condition, independent of whether subjects received fast (90°/s) or slow (60°/s) constant-velocity rotations. This latter finding suggests that both effects are functionally distinct and that the later effect is not sensitive to manipulation of suprathreshold (i.e. above perceptual threshold) stimulus intensity as tested here, reflecting a more general difference between vestibular activation and control conditions. Specifically, both fast and slow rotations were above the 5°/s perceptual threshold of vestibular rotation (Goldberg and Fernandez, 1971; Grabherr et al., 2008) and somatosensory activation was always above perceptual threshold (i.e. 3–4 times of perceptual threshold; see Methods). Our finding of two distinct topographical maps during the late period further corroborated these differences: one topographical map (Map 1) accounted more strongly for SEPs during vestibular activation and another one (Map 2) for the SEPs during the non-vestibular control condition.

The latency of this later effect (97–112 ms) may suggest involvement of the S2 as previously reported by surface (Waberski et al., 2002) and intracranial recordings (Allison et al., 1989b; Cullen, 2012; Garcia-Larrea et al., 1995). The human S2 region is located in the upper wall of the Sylvian fissure, thus somewhat more superior to the MTG region as revealed by our source estimation. Bearing in mind the limited spatial resolution of EEG, the limited number of electrodes (i.e. 64 electrodes) and the fact that a previous SEP study attributed MTG EEG activations in the same time period to functional processing in S2 (Waberski et al., 2002), and based on the cited intracranial human data (Allison, McCarthy, Wood, Williamson, et al., 1989), we argue that the late effect relates to neural generators in S2. Compatible with such a proposal, previous PET studies in humans found that vestibular activation and somatosensory activations showed overlapping modulation of brain activity in the S2, MTG and further regions of the temporoparietal junction (Bottini et al., 1994, 2001). We also note that S2 processes cutaneous and proprioceptive signals (Burton and Sinclair, 1991; Disbrow et al., 2003) and has reciprocal connections with both S1 and PIVC (Guldin et al., 1992; Guldin and Grüsser, 1998). In humans, CVS as well as neck-muscle vibration activated S2 (and the medial-posterior insula, putamen, and anterior cingulate cortex Bottini et al., 2001; Fasold et al., 2008). Thus, our data extends these PET and fMRI results showing that physiological vestibular activation modulates somatosensory processing in S2. Our results further extend a recent study by Ferrè et al. (2012) who reported vestibular modulation (using CVS) of SEPs and discussed this effect to putative S2 activation and also argued that such activity changes in the somatosensory cortex may underlie the perceptual effects of vestibular activation on tactile processing in neurological patients and healthy subjects (Bottini et al., 1995, 2005; Ferrè et al., 2011, 2013, 2014; Kerkhoff et al., 2011; Vallar et al., 1990). The present SEP data suggest that such effects may be caused by vestibular–somatosensory mechanisms in S1, S2, or the other regions described in the present study and that vestibular–somatosensory effects are present at least during two distinct (early and late) time periods. One might argue that the anatomical location of our MTG activation may rather indicate vestibular effects on multisensory stimulus attention. That is, previous neuroimaging studies found that the MTG also encodes attention capture due to changing patterns of somatosensory, visual, or auditory activation (Downar et al., 2000), auditory–visual changes in attention (Desimone and Duncan, 1995), and changes of spatial attention to body parts (Waberski et al., 2002). However, several PET, fMRI, as well as behavioral studies provided evidence for direct vestibular–somatosensory interactions independent of general attention effects (Bottini et al., 1994, 2001; Ferrè et al., 2011, 2013). Thus, although we cannot rule out that our MTG activation

Table 3
SEP waveform component summarized (CP4 electrode).

	Latency							Amplitude						
	N20 Lat. ms	P26 Lat. ms	N35 Lat. ms	P45 Lat. ms	N60 Lat. ms	P80 Lat. ms	N140 Lat. ms	N20-P26 Amp. mV	P26-N35 Amp. mV	N35-P45 Amp. mV	P45-N60 Amp. mV	N60-P80 Amp. mV	P80-N140 Amp. mV
Vest. fast	19.9 (1.6)	27.4 (2.8)	35.4 (2.8)	45.8 (5.1)	60.4 (6.2)	78.2 (7.4)	127.9 (10.4)	2.6 (1.6)	1.6 (1.0)	2.3 (1.2)	2.1 (1.2)	1.1 (0.8)	3.0 (1.1)
Vest. slow	19.7 (1.7)	27.3 (3.0)	35.6 (3.3)	46.3 (5.5)	61.0 (6.1)	77.0 (6.5)	127.3 (10.9)	2.7 (1.7)	1.6 (1.0)	2.2 (1.2)	2.1 (1.2)	1.1 (0.9)	3.2 (1.2)
Ctrl. fast	19.7 (1.3)	26.8 (3.1)	35.5 (3.2)	46.3 (5.8)	61.6 (6.8)	78.2 (6.4)	127.1 (11.6)	2.6 (1.5)	1.6 (0.9)	2.2 (1.2)	2.0 (1.2)	1.2 (0.7)	3.1 (1.4)
Ctrl. slow	19.6 (1.6)	27.8 (2.9)	36.0 (3.0)	45.9 (5.4)	59.2 (5.3)	76.8 (6.0)	127.1 (11.7)	2.6 (1.7)	1.6 (0.9)	2.1 (1.1)	2.1 (1.2)	1.1 (0.8)	3.1 (1.2)

Values are means; numbers in brackets are standard deviations; SEP, somatosensory evoked potential; Vest., vestibular activation condition; Ctrl., control condition.

reflects potential involvement of these multisensory attention-related regions, they are unlikely to underlie the temporal-specific vestibular effects on SEPs observed here.

Conclusion

Whereas in earlier human studies, vestibular–somatosensory interaction effects were based on artificial vestibular stimulations co-activating thermal, nociceptive, or acoustic receptors and related cortical representations (Lopez et al., 2012a) and using low temporal resolution neuroimaging techniques (Bense et al., 2001; Bottini et al., 1994), the combination of a motion platform with high-density EEG in the present study allowed us to measure brain responses to yaw rotations. We observed two distinct vestibular effects on somatosensory cortical processing induced in humans by yaw rotations. One early process involved activation of S1 (including vestibular areas 2v and 3a), the posterior insula, as well as precuneus and S2 and this effect was stronger for faster rotation speeds and associated with suppression of SEP global electrical field amplitude. Importantly, the same topographical EEG pattern was found across all four conditions (including non-vestibular control conditions). We also describe a later vestibular–somatosensory process that activated different brain regions in the vestibular versus non-vestibular conditions (showing topographical EEG differences) and this effect was independent of the rotation velocity. These results show that vestibular signals differently affect multiple processing stages in distinct and distributed somatosensory–vestibular cortical regions. Generally it is assumed that somatosensory signals are processed hierarchically, where early SEP components (<50 ms post-stimulus latency) reflect processing in S1 and S2 cortices (Allison et al., 1989a) and later SEP components (>50 ms) correspond to higher-order processing in fronto-parietal networks (Allison et al., 1989b). Accordingly, we propose that the effects observed in our study reflect that the first process serves to rapidly integrate vestibular signals with concurrent somatosensory inputs and that the second process serves to modulate higher-order somatosensory processing in fronto-parietal networks, possibly contributing to functions such as touch localization, tactile awareness, integration of bilateral body parts and of multisensory input (Ferrè et al., 2013; Iwamura, 1998; Lopez et al., 2010, 2012b; Pfeiffer et al., 2014). These electrophysiological results in humans are highly similar to observations in animal studies that several distinct and interconnected cortical areas host neurons that respond to vestibular and somatosensory simulation (Fredrickson et al., 1966; Grüsser et al., 1990b; Odkvist et al., 1974).

Grants

This work was supported by the Swiss National Science Foundation SINERGIA Grant CRSII1-125135, the European Science Foundation FP7 project VERE Grant No. 257695, and the Bertarelli Foundation to O. Blanke and the Netherlands Organization for Scientific Research VENI Grant No. 016.135.135 to M. v. Elk.

Disclosures

The authors declare that the research reported in this manuscript has been conducted in the absence of financial and commercial relationships that may be construed as a potential conflict of interest.

Acknowledgments

We thank E.R. Ferrè, M. de Lucia, and S. Marchesotti for helpful comments on methods and analyses.

Appendix A. *Complementary SEP waveform analysis*

A positive peak-activation channel was identified by calculating the group-average condition-average SEP over the 20–35 ms post-stimulus period, i.e. when the first cortical response to median nerve stimulation was expected (Allison et al., 1989a). As expected, this revealed the CP4 electrode in a posterior location on the right hemisphere approximately above the primary somatosensory cortex (Fig. 2A). Following the method by Schubert et al. (2006), positive and negative waveform voltage peaks were identified in the group-average time-wise data in the CP4 channel. All classical SEP components were observed, which depending on their polarity (i.e. N for negative, P for positive) and latency were denoted as N20, P26, N35, P45, N60, P80, and N140 components. Condition-wise component peak-latencies and peak-to-peak amplitudes were extracted by automated search within non-overlapping time-windows around the group average component peak. Search windows (in brackets) for each component were: N20 (18–22 ms), P26 (23–29 ms), N35 (30–40 ms), P45 (41–50 ms), N60 (51–70 ms), P80 (71–90 ms), and N140 (100–150 ms). Statistical analysis using separate 2×2 repeated measures ANOVAs was performed for peak-latencies and peak-to-peak amplitudes per SEP component (alpha threshold of 0.05, uncorrected for multiple comparisons).

As expected, the group-average SEPs showed highest amplitudes for the N20 component in fronto-parietal EEG channels that were placed contralateral to the stimulated median nerve. Fig. 2A illustrates typical SEP components that were observed at electrode CP4 over the contralateral somatosensory cortex (Cruccu et al., 2008). Table 3 summarizes the latencies and amplitudes for the different SEP components recorded at scalp electrode CP4. Visual inspection of component-wise group-average latencies and peak-to-peak amplitudes showed that standard median nerve SEPs were evoked during vestibular activation and control conditions. Component-wise statistical analysis by separate 2×2 ANOVAs for these SEP component latencies and amplitudes showed not significant differences (all p-values > 0.05).

References

Akbarian, S., Grüsser, O.J., Guldin, W.O., 1993. Corticofugal projections to the vestibular nuclei in squirrel monkeys: further evidence of multiple cortical vestibular fields. J. Comp. Neurol. 332 (1), 89–104. http://dx.doi.org/10.1002/cne.903320107.

Akbarian, S., Grüsser, O.J., Guldin, W.O., 1994. Corticofugal connections between the cerebral cortex and brainstem vestibular nuclei in the macaque monkey. J. Comp. Neurol. 339 (3), 421–437. http://dx.doi.org/10.1002/cne.903390309.

Allison, T., McCarthy, G., Wood, C.C., Darcey, T.M., Spencer, D.D., Williamson, P.D., 1989a. Human cortical potentials evoked by stimulation of the median nerve. I. Cytoarchitectonic areas generating short-latency activity. J. Neurophysiol. 62 (3), 694–710.

Allison, T., McCarthy, G., Wood, C.C., Williamson, P.D., Spencer, D.D., 1989b. Human cortical potentials evoked by stimulation of the median nerve. II. Cytoarchitectonic areas generating long-latency activity. J. Neurophysiol. 62 (3), 711–722.

Ary, J.P., Klein, S.A., Fender, D.H., 1981. Location of sources of evoked scalp potentials: corrections for skull and scalp thicknesses. IEEE Trans. Biomed. Eng. 28 (6), 447–452. http://dx.doi.org/10.1109/TBME.1981.324817.

Barresi, M., Grasso, C., Li Volsi, G., Manzoni, D., 2013. Effects of body to head rotation on the labyrinthine responses of rat vestibular neurons. Neuroscience 244, 134–146. http://dx.doi.org/10.1016/j.neuroscience.2013.04.010.

Bense, S., Stephan, T., Yousry, T.A., Brandt, T., Dieterich, M., 2001. Multisensory cortical signal increases and decreases during vestibular galvanic stimulation (fMRI). J. Neurophysiol. 85 (2), 886–899.

Bernasconi, F., De Lucia, M., Tzovara, A., Manuel, A.L., Murray, M.M., Spierer, L., 2011. Noise in brain activity engenders perception and influences discrimination sensitivity. J. Neurosci. 31 (49), 17971–17981. http://dx.doi.org/10.1523/JNEUROSCI.3715-11.2011.

Berthoz, A., 1991. Reference frames for the perception and control of movement. In: Paillard, J. (Ed.), Brain and Space. Oxford University Press, New York, pp. 81–111.

Bertolini, G., Bockisch, C.J., Straumann, D., Zee, D.S., Ramat, S., 2008. Estimating the time constant of pitch rVOR by separation of otoliths and semicircular canals contributions. Conference Proceedings: IEEE Engineering in Medicine and Biology Society, 2008, pp. 1060–1063 http://dx.doi.org/10.1109/IEMBS.2008.4649342.

Bertolini, G., Ramat, S., Laurens, J., Bockisch, C.J., Marti, S., Straumann, D., Palla, A., 2011. Velocity storage contribution to vestibular self-motion perception in healthy human subjects. J. Neurophysiol. 105 (1), 209–223. http://dx.doi.org/10.1152/jn.00154.2010.

Blanke, O., Perrig, S., Thut, G., Landis, T., Seeck, M., 2000. Simple and complex vestibular responses induced by electrical cortical stimulation of the parietal cortex in humans. J. Neurol. Neurosurg. Psychiatry 69 (4), 553–556.
Blanke, O., Ortigue, S., Landis, T., Seeck, M., 2002. Stimulating illusory own-body perceptions. Nature 419 (6904), 269–270. http://dx.doi.org/10.1038/419269a.
Bottini, G., Sterzi, R., Paulesu, E., Vallar, G., Cappa, S.F., Erminio, F., ... Frackowiak, R.S., 1994. Identification of the central vestibular projections in man: a positron emission tomography activation study. Exp. Brain Res. 99 (1), 164–169.
Bottini, G., Paulesu, E., Sterzi, R., Warburton, E., Wise, R.J., Vallar, G., ... Frith, C.D., 1995. Modulation of conscious experience by peripheral sensory stimuli. Nature 376 (6543), 778–781. http://dx.doi.org/10.1038/376778a0.
Bottini, G., Karnath, H.O., Vallar, G., Sterzi, R., Frith, C.D., Frackowiak, R.S., Paulesu, E., 2001. Cerebral representations for egocentric space: functional–anatomical evidence from caloric vestibular stimulation and neck vibration. Brain 124 (Pt 6), 1182–1196.
Bottini, G., Paulesu, E., Gandola, M., Loffredo, S., Scarpa, P., Sterzi, R., ... Vallar, G., 2005. Left caloric vestibular stimulation ameliorates right hemianesthesia. Neurology 65 (8), 1278–1283. http://dx.doi.org/10.1212/01.wnl.0000182398.14088.e8.
Brandt, T., Strupp, M., Dieterich, M., 2014. Towards a concept of disorders of "higher vestibular function". Front. Integr. Neurosci. 8, 47. http://dx.doi.org/10.3389/fnint.2014.00047.
Bremmer, F., Klam, F., Duhamel, J.R., Ben Hamed, S., Graf, W., 2002. Visual–vestibular interactive responses in the macaque ventral intraparietal area (VIP). Eur. J. Neurosci. 16 (8), 1569–1586.
Burton, H., Sinclair, R.J., 1991. Second somatosensory cortical area in macaque monkeys: 2. Neuronal responses to punctate vibrotactile stimulation of glabrous skin on the hand. Brain Res. 538 (1), 127–135.
Büttner, U., Buettner, U.W., 1978. Parietal cortex (2v) neuronal activity in the alert monkey during natural vestibular and optokinetic stimulation. Brain Res. 153 (2), 392–397.
Büttner, U., Waespe, W., 1981. Vestibular nerve activity in the alert monkey during vestibular and optokinetic nystagmus. Exp. Brain Res. 41 (3–4), 310–315.
Cavanna, A.E., Trimble, M.R., 2006. The precuneus: a review of its functional anatomy and behavioural correlates. Brain 129 (Pt 3), 564–583. http://dx.doi.org/10.1093/brain/awl004.
Chen, A., DeAngelis, G.C., Angelaki, D.E., 2010. Macaque parieto-insular vestibular cortex: responses to self-motion and optic flow. J. Neurosci. 30 (8), 3022–3042. http://dx.doi.org/10.1523/JNEUROSCI.4029-09.2010.
Cohen, B., Henn, V., Raphan, T., Dennett, D., 1981. Velocity storage, nystagmus, and visual–vestibular interactions in humans. Ann. N. Y. Acad. Sci. 374, 421–433.
Cruccu, G., Aminoff, M.J., Curio, G., Guerit, J.M., Kakigi, R., Mauguiere, F., ... Garcia-Larrea, L., 2008. Recommendations for the clinical use of somatosensory-evoked potentials. Clin. Neurophysiol. 119 (8), 1705–1719. http://dx.doi.org/10.1016/j.clinph.2008.03.016.
Cullen, K.E., 2012. The vestibular system: multimodal integration and encoding of self-motion for motor control. Trends Neurosci. 35 (3), 185–196. http://dx.doi.org/10.1016/j.tins.2011.12.001.
Day, B.L., Fitzpatrick, R.C., 2005. Virtual head rotation reveals a process of route reconstruction from human vestibular signals. J. Physiol. 567 (Pt 2), 591–597. http://dx.doi.org/10.1113/jphysiol.2005.092544.
Desimone, R., Duncan, J., 1995. Neural mechanisms of selective visual attention. Annu. Rev. Neurosci. 18, 193–222. http://dx.doi.org/10.1146/annurev.ne.18.030195.001205.
Dieterich, M., Brandt, T., 2015. The bilateral central vestibular system: its pathways, functions, and disorders. Ann. N. Y. Acad. Sci. http://dx.doi.org/10.1111/nyas.12585.
Dieterich, M., Bense, S., Lutz, S., Drzezga, A., Stephan, T., Bartenstein, P., Brandt, T., 2003. Dominance for vestibular cortical function in the non-dominant hemisphere. Cereb. Cortex 13 (9), 994–1007.
Disbrow, E., Litinas, E., Recanzone, G.H., Padberg, J., Krubitzer, L., 2003. Cortical connections of the second somatosensory area and the parietal ventral area in macaque monkeys. J. Comp. Neurol. 462 (4), 382–399. http://dx.doi.org/10.1002/cne.10731.
Downar, J., Crawley, A.P., Mikulis, D.J., Davis, K.D., 2000. A multimodal cortical network for the detection of changes in the sensory environment. Nat. Neurosci. 3 (3), 277–283. http://dx.doi.org/10.1038/72991.
Duffy, C.J., 1998. MST neurons respond to optic flow and translational movement. J. Neurophysiol. 80 (4), 1816–1827.
Fasold, O., von Brevern, M., Kuhberg, M., Ploner, C.J., Villringer, A., Lempert, T., Wenzel, R., 2002. Human vestibular cortex as identified with caloric stimulation in functional magnetic resonance imaging. NeuroImage 17 (3), 1384–1393.
Fasold, O., Heinau, J., Trenner, M.U., Villringer, A., Wenzel, R., 2008. Proprioceptive head posture-related processing in human polysensory cortical areas. NeuroImage 40 (3), 1232–1242. http://dx.doi.org/10.1016/j.neuroimage.2007.12.060.
Ferrè, E.R., Bottini, G., Haggard, P., 2011. Vestibular modulation of somatosensory perception. Eur. J. Neurosci. 34 (8), 1337–1344. http://dx.doi.org/10.1111/j.1460-9568.2011.07859.x.
Ferrè, E.R., Bottini, G., Haggard, P., 2012. Vestibular inputs modulate somatosensory cortical processing. Brain Struct. Funct. 217 (4), 859–864. http://dx.doi.org/10.1007/s00429-012-0404-7.
Ferrè, E.R., Day, B.L., Bottini, G., Haggard, P., 2013. How the vestibular system interacts with somatosensory perception: a sham-controlled study with galvanic vestibular stimulation. Neurosci. Lett. 550, 35–40. http://dx.doi.org/10.1016/j.neulet.2013.06.046.
Ferrè, E.R., Vagnoni, E., Haggard, P., 2013. Vestibular contributions to bodily awareness. Neuropsychologia 51 (8), 1445–1452. http://dx.doi.org/10.1016/j.neuropsychologia.2013.04.006.
Ferrè, E.R., Kaliuzhna, M., Herbelin, B., Haggard, P., Blanke, O., 2014. Vestibular–somatosensory interactions: effects of passive whole-body rotation on somatosensory detection. PLoS One 9 (1), e86379. http://dx.doi.org/10.1371/journal.pone.0086379.
Fetsch, C.R., Wang, S., Gu, Y., Deangelis, G.C., Angelaki, D.E., 2007. Spatial reference frames of visual, vestibular, and multimodal heading signals in the dorsal subdivision of the medial superior temporal area. J. Neurosci. 27 (3), 700–712. http://dx.doi.org/10.1523/JNEUROSCI.3553-06.2007.
Fredrickson, J.M., Scheid, P., Figge, U., Kornhuber, H.H., 1966. Vestibular nerve projection to the cerebral cortex of the rhesus monkey. Exp. Brain Res. 2 (4), 318–327.
Garcia-Larrea, L., Lukaszewicz, A.C., Mauguiere, F., 1995. Somatosensory responses during selective spatial attention: the N120-to-N140 transition. Psychophysiology 32 (6), 526–537.
Goldberg, J.M., Fernandez, C., 1971. Physiology of peripheral neurons innervating semicircular canals of the squirrel monkey. I. Resting discharge and response to constant angular accelerations. J. Neurophysiol. 34 (4), 635–660.
Grabherr, L., Nicoucar, K., Mast, F.W., Merfeld, D.M., 2008. Vestibular thresholds for yaw rotation about an earth-vertical axis as a function of frequency. Exp. Brain Res. 186 (4), 677–681. http://dx.doi.org/10.1007/s00221-008-1350-8.
Grave de Peralta Menendez, R., Gonzalez Andino, S., Lantz, G., Michel, C.M., Landis, T., 2001. Noninvasive localization of electromagnetic epileptic activity. I. Method descriptions and simulations. Brain Topogr. 14 (2), 131–137.
Grüsser, O.J., Pause, M., Schreiter, U., 1990a. Localization and responses of neurones in the parieto-insular vestibular cortex of awake monkeys (*Macaca fascicularis*). J. Physiol. 430, 537–557.
Grüsser, O.J., Pause, M., Schreiter, U., 1990b. Vestibular neurones in the parieto-insular cortex of monkeys (*Macaca fascicularis*): visual and neck receptor responses. J. Physiol. 430, 559–583.
Guldin, W.O., Grüsser, O.J., 1998. Is there a vestibular cortex? Trends Neurosci. 21 (6), 254–259.
Guldin, W.O., Akbarian, S., Grüsser, O.J., 1992. Cortico-cortical connections and cytoarchitectonics of the primate vestibular cortex: a study in squirrel monkeys (*Saimiri sciureus*). J. Comp. Neurol. 326 (3), 375–401. http://dx.doi.org/10.1002/cne.903260306.
Guthrie, D., Buchwald, J.S., 1991. Significance testing of difference potentials. Psychophysiology 28 (2), 240–244.
Heydrich, L., Dieguez, S., Grunwald, T., Seeck, M., Blanke, O., 2010. Illusory own body perceptions: case reports and relevance for bodily self-consciousness. Conscious. Cogn. 19 (3), 702–710. http://dx.doi.org/10.1016/j.concog.2010.04.010.
Iwamura, Y., 1998. Hierarchical somatosensory processing. Curr. Opin. Neurobiol. 8 (4), 522–528.
Johansson, R., Magnusson, M., 1991. Human postural dynamics. Crit. Rev. Biomed. Eng. 18 (6), 413–437.
Kerkhoff, G., Hildebrandt, H., Reinhart, S., Kardinal, M., Dimova, V., Utz, K.S., 2011. A long-lasting improvement of tactile extinction after galvanic vestibular stimulation: two sham-stimulation controlled case studies. Neuropsychologia 49 (2), 186–195. http://dx.doi.org/10.1016/j.neuropsychologia.2010.11.014.
Koenig, T., Melie-Garcia, L., 2010. A method to determine the presence of averaged event-related fields using randomization tests. Brain Topogr. 23 (3), 233–242. http://dx.doi.org/10.1007/s10548-010-0142-1.
Lacour, M., Barthelemy, J., Borel, L., Magnan, J., Xerri, C., Chays, A., Ouaknine, M., 1997. Sensory strategies in human postural control before and after unilateral vestibular neurotomy. Exp. Brain Res. 115 (2), 300–310.
Laurens, J., Angelaki, D.E., 2011. The functional significance of velocity storage and its dependence on gravity. Exp. Brain Res. 210 (3–4), 407–422. http://dx.doi.org/10.1007/s00221-011-2568-4.
Laurens, J., Meng, H., Angelaki, D.E., 2013. Computation of linear acceleration through an internal model in the macaque cerebellum. Nat. Neurosci. 16 (11), 1701–1708. http://dx.doi.org/10.1038/nn.3530.
Lehmann, D., Skrandies, W., 1980. Reference-free identification of components of checkerboard-evoked multichannel potential fields. Electroencephalogr. Clin. Neurophysiol. 48 (6), 609–621.
Lobel, E., Kleine, J.F., Bihan, D.L., Leroy-Willig, A., Berthoz, A., 1998. Functional MRI of galvanic vestibular stimulation. J. Neurophysiol. 80 (5), 2699–2709.
Lopez, C., Blanke, O., 2011. The thalamocortical vestibular system in animals and humans. Brain Res. Rev. 67 (1–2), 119–146. http://dx.doi.org/10.1016/j.brainresrev.2010.12.002.
Lopez, C., Lenggenhager, B., Blanke, O., 2010. How vestibular stimulation interacts with illusory hand ownership. Conscious. Cogn. 19 (1), 33–47. http://dx.doi.org/10.1016/j.concog.2009.12.003.
Lopez, C., Blanke, O., Mast, F.W., 2012a. The human vestibular cortex revealed by coordinate-based activation likelihood estimation meta-analysis. Neuroscience 212, 159–179. http://dx.doi.org/10.1016/j.neuroscience.2012.03.028.
Lopez, C., Schreyer, H.-M., Preuss, N., Mast, F.W., 2012b. Vestibular stimulation modifies the body schema. Neuropsychologia 50 (8), 1830–1837. http://dx.doi.org/10.1016/j.neuropsychologia.2012.04.008.
MacNeilage, P.R., Banks, M.S., Berger, D.R., Bulthoff, H.H., 2007. A Bayesian model of the disambiguation of gravitoinertial force by visual cues. Exp. Brain Res. 179 (2), 263–290. http://dx.doi.org/10.1007/s00221-006-0792-0.
Margulies, D.S., Vincent, J.L., Kelly, C., Lohmann, G., Uddin, L.Q., Biswal, B.B., ... Petrides, M., 2009. Precuneus shares intrinsic functional architecture in humans and monkeys. Proc. Natl. Acad. Sci. 106 (47), 20069–20074. http://dx.doi.org/10.1073/pnas.0905314106.
Mauguiere, F., 2005. Somatosensory evoked potentials: normal responses, abnormal waveforms, and clinical applications in neurological diseases. ElectroencephalographyLippincott William & Wilkins, Philadelphia.
Mazzola, L., Lopez, C., Faillenot, I., Chouchou, F., Mauguiere, F., Isnard, J., 2014. Vestibular responses to direct stimulation of the human insular cortex. Ann. Neurol. 76 (4), 609–619. http://dx.doi.org/10.1002/ana.24252.
Michel, C.M., Murray, M.M., Lantz, G., Gonzalez, S., Spinelli, L., Grave de Peralta, R., 2004. EEG source imaging. Clin. Neurophysiol. 115 (10), 2195–2222. http://dx.doi.org/10.1016/j.clinph.2004.06.001.

Murray, M.M., Brunet, D., Michel, C.M., 2008. Topographic ERP analyses: a step-by-step tutorial review. Brain Topogr. 20 (4), 249–264. http://dx.doi.org/10.1007/s10548-008-0054-5.

Nolan, H., Whelan, R., Reilly, R.B., 2010. FASTER: fully automated statistical thresholding for EEG artifact rejection. J. Neurosci. Methods 192 (1), 152–162. http://dx.doi.org/10.1016/j.jneumeth.2010.07.015.

Odkvist, L.M., Schwarz, D.W., Fredrickson, J.M., Hassler, R., 1974. Projection of the vestibular nerve to the area 3a arm field in the squirrel monkey (*Saimiri sciureus*). Exp. Brain Res. 21 (1), 97–105.

Pascual-Marqui, R.D., Michel, C.M., Lehmann, D., 1995. Segmentation of brain electrical activity into microstates: model estimation and validation. IEEE Trans. Biomed. Eng. 42 (7), 658–665. http://dx.doi.org/10.1109/10.391164.

Penfield, W., Jaspers, H., 1954. Epilepsy and the Functional Anatomy of the Human Brain. Little Brown & Co., Boston.

Pfeiffer, C., Serino, A., Blanke, O., 2014. The vestibular system: a spatial reference for bodily self-consciousness. Front. Integr. Neurosci. http://dx.doi.org/10.3389/fnint.2014.00031.

Prsa, M., Gale, S., Blanke, O., 2012. Self-motion leads to mandatory cue fusion across sensory modalities. J. Neurophysiol. 108 (8), 2282–2291. http://dx.doi.org/10.1152/jn.00439.2012.

Raphan, T., Matsuo, V., Cohen, B., 1979. Velocity storage in the vestibulo-ocular reflex arc (VOR). Exp. Brain Res. 35 (2), 229–248.

Roberts, D.C., Marcelli, V., Gillen, J.S., Carey, J.P., Della Santina, C.C., Zee, D.S., 2011. MRI magnetic field stimulates rotational sensors of the brain. Curr. Biol. 21 (19), 1635–1640. http://dx.doi.org/10.1016/j.cub.2011.08.029.

Schlack, A., Hoffmann, K.P., Bremmer, F., 2002. Interaction of linear vestibular and visual stimulation in the macaque ventral intraparietal area (VIP). Eur. J. Neurosci. 16 (10), 1877–1886.

Schubert, R., Blankenburg, F., Lemm, S., Villringer, A., Curio, G., 2006. Now you feel it—now you don't: ERP correlates of somatosensory awareness. Psychophysiology 43 (1), 31–40. http://dx.doi.org/10.1111/j.1469-8986.2006.00379.x.

Schwarz, D.W., Fredrickson, J.M., 1971. Rhesus monkey vestibular cortex: a bimodal primary projection field. Science 172 (3980), 280–281.

Spinelli, L., Andino, S.G., Lantz, G., Seeck, M., Michel, C.M., 2000. Electromagnetic inverse solutions in anatomically constrained spherical head models. Brain Topogr. 13 (2), 115–125.

Suzuki, M., Kitano, H., Ito, R., Kitanishi, T., Yazawa, Y., Ogawa, T., ... Kitajima, K., 2001. Cortical and subcortical vestibular response to caloric stimulation detected by functional magnetic resonance imaging. Brain Res. Cogn. Brain Res. 12 (3), 441–449.

Talairach, J., Tournoux, P., 1988. Co-planar Stereotaxic Atlas of the Human Brain. Thieme, New York.

Vallar, G., Sterzi, R., Bottini, G., Cappa, S., Rusconi, M.L., 1990. Temporary remission of left hemianesthesia after vestibular stimulation. A sensory neglect phenomenon. Cortex 26 (1), 123–131.

van Elk, M., Blanke, O., 2013. Imagined own-body transformations during passive self-motion. Psychological Research http://dx.doi.org/10.1007/s00426-013-0486-8.

Vogt, B.A., Pandya, D.N., 1978. Cortico-cortical connections of somatic sensory cortex (areas 3, 1 and 2) in the rhesus monkey. J. Comp. Neurol. 177 (2), 179–191. http://dx.doi.org/10.1002/cne.901770202.

Waberski, T.D., Gobbele, R., Darvas, F., Schmitz, S., Buchner, H., 2002. Spatiotemporal imaging of electrical activity related to attention to somatosensory stimulation. NeuroImage 17 (3), 1347–1357.

Waespe, W., Henn, V., Isoviita, V., 1980. Nystagmus slow-phase velocity during vestibular, optokinetic, and combined stimulation in the monkey. Arch. Psychiatr. Nervenkr. 228 (4), 275–286.

zu Eulenburg, P., Caspers, S., Roski, C., Eickhoff, S.B., 2012. Meta-analytical definition and functional connectivity of the human vestibular cortex. NeuroImage 60 (1), 162–169. http://dx.doi.org/10.1016/j.neuroimage.2011.12.032.